Funneled focusing of planar acoustic waves utilizing the metamaterial properties of an acoustic lens

E. Walker[a], D. Reyes[b], M.M. Rojas[b], A. Krokhin[a], A. Neogi[a]

[a]Dept. of Physics, University of North Texas, 210 Avenue A., Denton, TX USA 76201-1427
[b]Universidad Autónoma del Estado de México, Toluca, 50120 , Mexico

ABSTRACT

Metamaterial acoustic lenses are acoustic devices based on phononic crystal structures that take advantage of negative or near-zero indices of refraction. These unique properties arise due to either the antiparallel direction of the phase and group velocity or strongly anisotropic dispersion characteristics, usually above the first transmission band. In this study, we utilize an FDTD program to examine two phononic lenses that utilize anisotropic effects available in their second band to collimate and focus acoustic waves from a plane-wave source with a k_{00} wavevector. The phononic crystals consist of stainless steel rods arranged in a square lattice with water as the ambient material. Results show collimation and focusing in the second band for select frequencies, $f_c \pm 0.005 f_c$.

Keywords: Metamaterial, phononic crystal, ultrasonic lens, references

1. INTRODUCTION

The history of metamaterials can be traced back to the work of Veselago and the exploration of the feasibility of simultaneously negative permeability and permittivity in dielectrics [1]. Such materials exhibit left-handedness that is not observed in nature and results in peculiar effects such as negative index of refraction materials amongst other things [2, 3, 4, 5, 6]. However, there are no known materials that innately possess both negative permeability and permittivity, so the practical realization of such a material only occurred after the evolution of the effective medium theory for photonic crystals. Pendry et. al first demonstrated a metamaterial with a structure that possessed both negative permittivity and permeability through a periodic arrangement of metals [7]. Since that point, work pertaining to photonic metamaterials has grown exponentially with devices ranging from electromagnetic cloaks [8] to lenses that resolve beyond the diffraction limit [9, 10] realized both in theory and experiment.

The underlying concepts of photonic crystals and the propagation of electronic or electromagnetic waves through an ordered lattice are readily applicable to the propagation of mechanical waves through a similarly ordered lattice [11, 12]. Permittivity and permeability become analogous to Lamé's first parameter and inverse density leading to, roughly, the substitution of the physical material properties such as the density contrast, sound velocity, and attenuation, for the dielectric properties. For mechanical waves, however, the primary propagation mode being longitudinal, the ability of solids to support both longitudinal and transverse modes, and the lack of an innately negative density translates to some variation between the behavior of electromagnetic and mechanical waves in ordered structures. So, though the development of metamaterials was realized first using photonic crystals, the applications to phononic crystals were quickly realized and similar devices such as cloaks [13, 14] and negative index lenses [15, 16] have been demonstrated both theoretically and experimentally.

Critical to the realization of a metamaterial for either type of wave is a dispersion relation that does not follow the usually linearly increasing type found in the long wavelength limit for periodic structures [17, 18, 19, 20, 21]. The peculiar effects of metamaterials arise from the application of a periodic structure in a frequency region where the dispersion relation is either non-linear, anisotropic, or anomalous [22]. In photonic and phononic crystals, negative effective indices of refraction are realized by utilizing the crystal at a frequency where the dispersion curve has a negative slope. These conditions occur near the band edge of the first Brillouin zone [19], or in the second transmission band where band folding can result in antiparallel direction between the wavevector and Poynting vector [12, 19].

This work is particularly interested in the application of a 2D phononic crystal as a collimating lens for sound wave propagating in the plane of periodicity. The first transmission band of a periodic structure can be readily used to form an effective lens with basic geometric optics [20, 21]. However, as the frequency of the impinging wave increases, the dimensions of the structure, such as the size and spacing of the scatterers in a periodic lattice, must decrease appropriately. For this reason, lenses that operate in the second transmission band are of great interest because of the decreased difficulty in the practical realization of the structure. Lenses that operate in the second transmission band are metamaterial lenses. Studies, both theoretical and experimental, have clearly shown the focusing ability of metamaterial phononic lenses [23, 24]. Many are sourced by an approximate point source emission. Here, we present a theoretical demonstration of two phononic lenses that collimate ultrasonic k_{00} plane waves in their second band onto their optical axis.
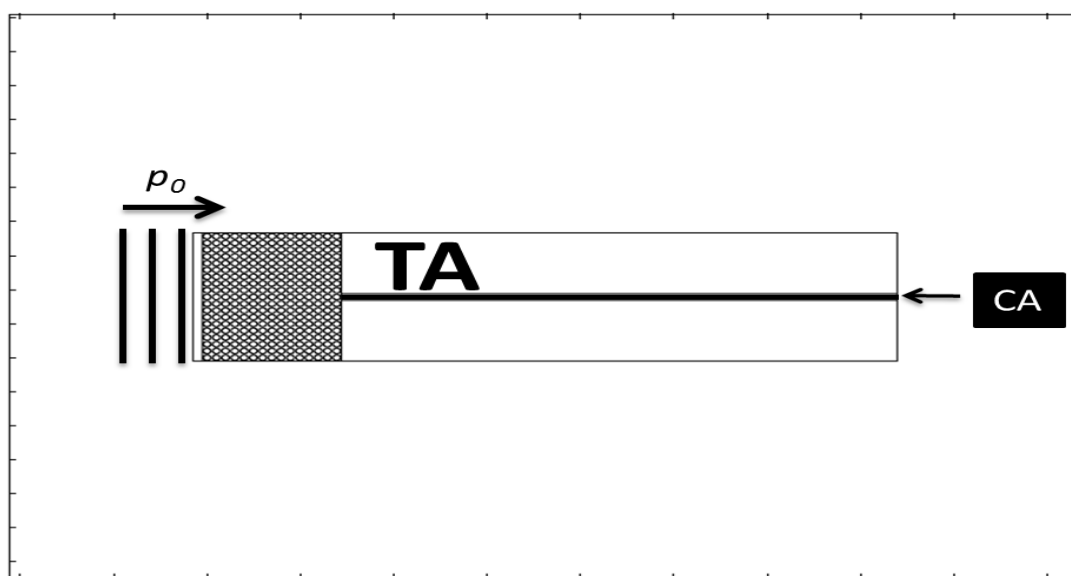
2. METHODOLOGY

Figure 1 - Illustration of the simulation setup using COMSOL 4.2. Propagating pressure waves starts from the left, is scattered by the phononic crystal, and measurements are recorded in the transmitted ares (TA) and collimating axis (CA).

For this study, we utilized the tools of COMSOL 4.2, an FDTD simulation program, to examine the collimating properties of two phononic crystal lenses: one of triangular shape, and the other a hemispherical. The lenses are based on a phononic crystal composed of 1.6 mm diameter stainless steel rods in water arranged in a *15 x 19* (*r x z*) square lattice with a lattice constant of 2 mm. Figure 1 illustrates the basic phononic crystal simulation setup. An initial pressure wave, p_0, is sourced on the opposite side of the area used for analysis. **TA** represents the entire transmission area, and is broken down in the analysis into two subsections. **CA** is the collimation (optical) axis of width of one lattice constant (2 mm) represented by the black strip in the center of **TA** in Figure 1. Scattered sound pressure levels (**SPL**) in specified portions of the region are used to determine the resulting behavior of the propagating pressure field. Simulations are carried out with a longitudinal k_{00} pressure wave, and the transmission bandstructure is determined by the average scattered SPL in the transmitted area, **TA**. The system is considered open as the boundaries of the simulation are set to perfectly absorb all radiation that would exit the region. Collimation is determined by comparison of the SPL in **CA** to that outside of **CA**, fluctuations of the SPL as measured by probes along **CA**, and aided visually by the inspection of 2-D scattered SPL surface plots.

For this work, collimation is defined as the focusing and collimation of the transmitted pressure wave onto the optical axis. Collimation about the optical axis for the each lens is determined by comparison of the average SPL inside **CA** to the average SPL outside **CA**, an indicator collimating score determined for each frequency, and visual inspection of the simulated scattered SPL. Larger differences between the average SPL inside/outside **CA** are indicative of a collimation as it results higher transmitted pressure being scattered onto the optical axis versus outside it. The collimating score is determined from SPL probes situated at nine distances along the optical axis: 0 mm, 10 mm, 20 mm, 30 mm, 40 mm, 50 mm, 60 mm, 90 mm, 120 mm. The total distance amounts to $>40\lambda$ for all frequencies in the second transmission band. The collimating score is based on the following

$$C_f = \frac{\sigma_{CA}}{\Delta\bar{\xi}} + \frac{\delta\xi_{CA}}{\overline{\xi_{ca}}},$$

(1)

Where

$$\sigma_{CA} = standard\ deviation\ of\ SPL\ in\ CA,$$
$$\Delta\bar{\xi} = average\ SPL\ in\ CA - average\ SPL\ out\ CA$$
$$\delta\xi_{CA} = maximum\ SPL\ in\ CA - minimum\ SPL\ in\ CA,$$
$$\overline{\xi_{CA}} = average\ SPL\ in\ CA.$$

The collimation score is used as an indicator for frequency candidates with collimation characteristics along the optical axis in a transmission band. A collimating score of zero in a transmission band would constitute complete focusing and collimating of the pressure wave onto the optical axis. So, scores that are positive and nearest to zero indicate higher collimation and thus the best scores. Negative scores occur when a combination of the maximum and average SPLs outside **CA** are higher than inside **CA,** and thus represent frequencies that are highly dispersed by the lens; an undesired trait. Negative scores are represented in this analysis as collimation scores an order of magnitude larger than the worst score that does have a desirable collimating trait. The best collimating scores are used as the indicators of the frequencies that are collimating onto the optical axis, but are confirmed through additional visual inspection of the scattered SPL.
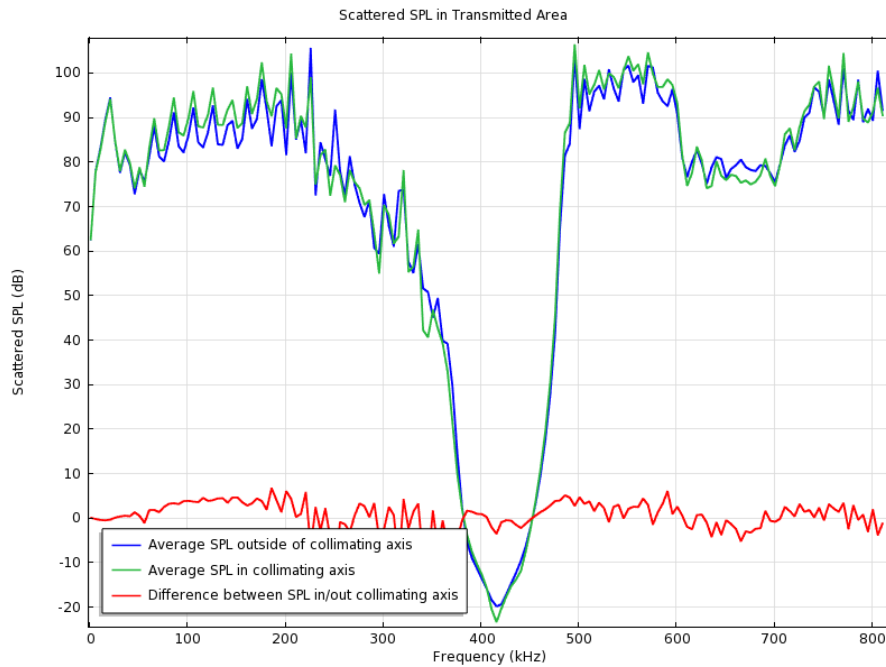
3. DATA

Figure 2 - k$_{00}$ transmission band structure from scattered average SPL. Transmission bandgap occurs between 390-460 kHz, with the second transmission band beginning at 485 kHz.

3.1 – 15 x 19 Phononic crystal

For wavelength,λ and lattice spacing, a, $(\lambda \gg a)$ the dispersion curve is linear and scattering cross-section is isotropic [22]. As $\lambda \to a$, the dispersion curve becomes non-linear and anisotropy occurs, with the strength of the anisotropy dependent on the non-linearity. The basis of the metamaterial collimating lens is the effectiveness of the lens for a k_{00} wave at a frequency, or small subset of frequencies, in the second transmission band where anisotropy readily occurs. Figure 2 shows the transmission spectrum based on the average scattered SPL in TA. The first transmission band extends to 230 kHz before tapering sharply to a stop-band from 390 – 460 kHz. The second transmission band, the focus of this work, starts at 485 kHz and continues to 590 kHz where another partial transmission reduction occurs. Important for implications in the collimating lens is the comparison between the SPL inside and outside the optical axis. The difference between the scattered SPL inside and outside the collimating axis, illustrated by the red line in Figure 2, shows minimal variation between SPL in the two regions with small differences arising as the frequency increases.
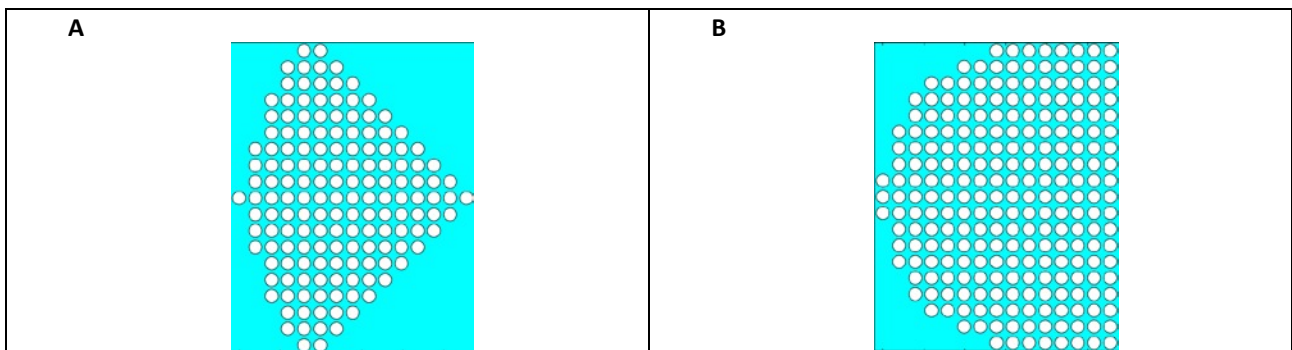

Figure 3 - Triangular arrowhead lens (A). Hemisphere lens (B). Both are based on 15 x 19 phononic crystal.

Many phononic metamaterial lenses utilize gradient indices by manipulating the hylemorphic properties of the periodic structure, specifically, the lattice spacing and scatterer size [4, 9, 18, 24]. Two lenses were investigated as part of this work. Both are based on the 15 x 19 square lattice phononic crystal geometrically shaped into a hemisphere and triangular arrowhead. The scatterers of the lens are stainless steel, and the effective medium is water at room temperature. No defects or lattice manipulations were utilized to enhance or manipulate wave propagation through the lens. Additionally, the scatterers are fixed so that there is no deformation in the lattice as a result of the impinging wave.

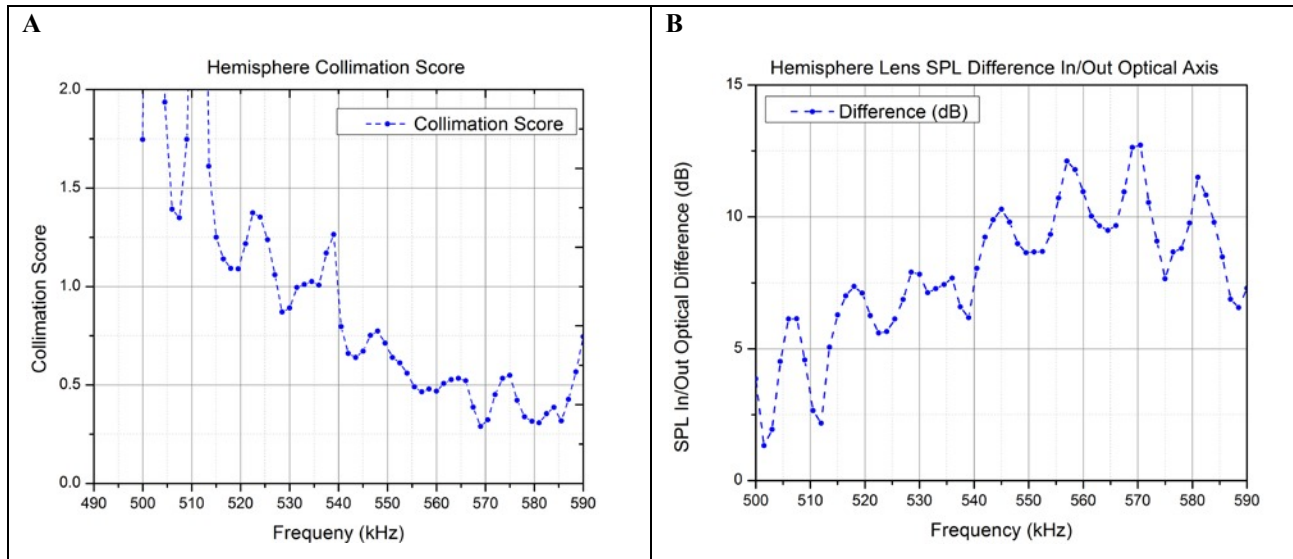## 3.2 – Lenses

Hemisphere Lens

Figure 4 - Collimation score (A) and difference in average SPL inside/outside CA (B) of the hemisphere collimation lens shown above.

Collimation for the hemisphere lens generally improves as frequency increases with a peak collimation score of 0.289 at 569 kHz. Other peak frequencies are 570 kHz and 581 kHz comparable values at 0.324 and 0.307 respectively. Movement off the peak frequency by 2.5 kHz results in an increase of the collimation score of 80% illustrating the frequency sensitivity of the focusing ability. The difference in the average SPL inside and outside the collimation axis also generally increases as frequency increases with a peak of 11.9 dB at 570 kHz. However, the values of the SPL variation do not sufficient represent the collimating ability of the lens as noted by the relatively high variation even at frequencies lower in the transmission band where the collimation score is definitively worse. Figure 6 A and Figure 6 C are images the scattered SPL of the hemisphere lens at 569 kHz and 514 kHz respectively. Though the SPL variation is 6 dB at 514 kHz, the collimation score of 1.61 indicates that collimation is comparatively weak as can been clearly seen in Figure 6 C.
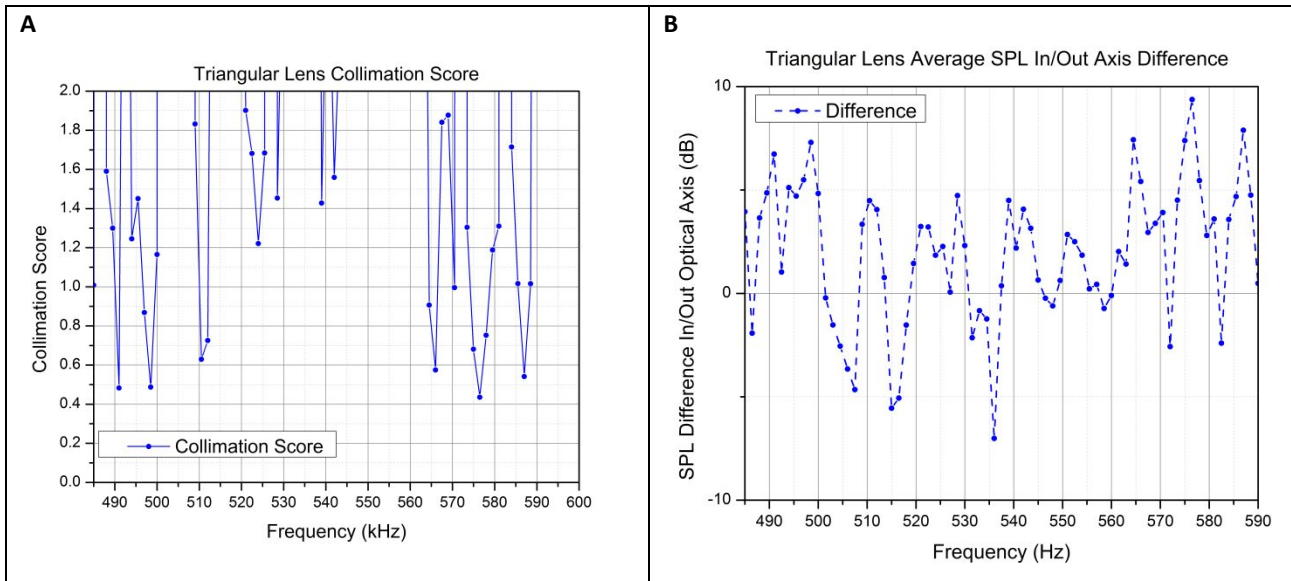
Figure 5 - Triangular lens collimation score (A) and SPL difference in/out CA (B). Behavior of both collimation score and SPL variation is due to the single initial scattering cell vs. three for the hemisphere lens

The triangular arrowhead lens displays much more erratic behavior compared to the hemisphere lens. The hemisphere lens possesses a flat surface at the impinging edge of the lens due to its curvature. The flat surface behaves that is 3a wide moderates the transmitted pressure wave similar to a 15 x 3 un-manipulated phononic crystal. This flat surface is non-existent in the triangular lens, allowing for more variation in the scattering of the initial pressure wave. The resulting effects of the variation in scattering can be seen in the SPL variation inside and outside the optical axis. Figure 5B illustrates this variation as many frequencies have a negative SPL difference, meaning that the average pressure outside the optical axis is higher than inside the optical axis. The collimation score follows similarly erratic behavior for the same reasons.

The peak collimation frequency for the triangular lens is 576 kHz with a collimation score of 0.435 (Figure 5A). The triangular lens has increased frequency sensitivity for effective collimation as compared to the hemisphere lens. A change of 1.5 kHz will increase in the collimation score 56%, while 2.5 kHz increases over 190%. 576 kHz is also the peak frequency for the positive variation in the in/out optical axis SPL (9.38 dB). Figure 6B and 6D are images of the scattered SPL at 576 kHz, where collimation occurs, and 560 kHz, where no collimation is apparent.
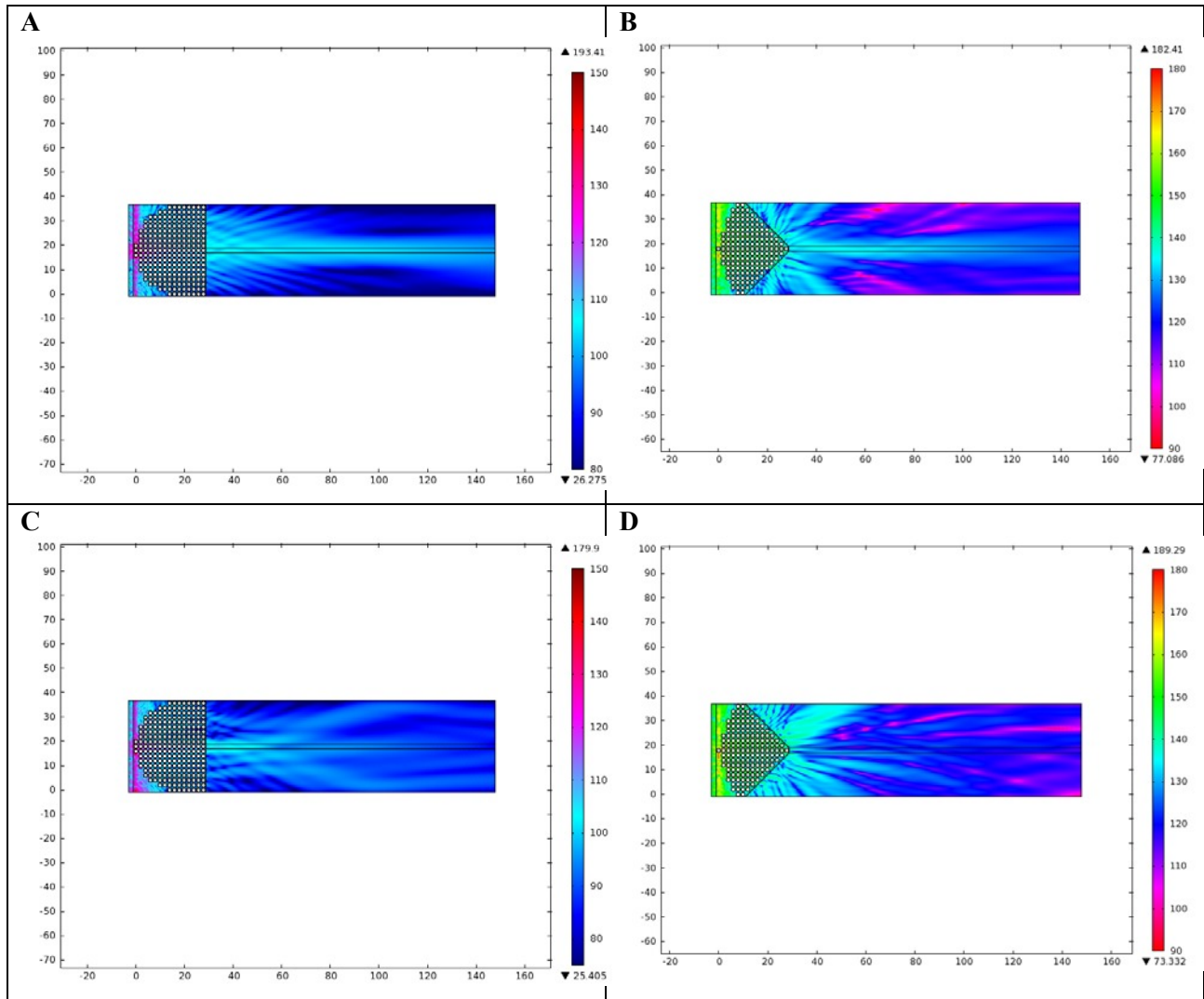
Figure 6 - A) SPL collimation in hemisphere lens at 569 kHz. B) SPL collimation in triangular lens at 576 kHz. C) SPL at high collimation score frequency 513 kHz for hemisphere lens. D) SPL for triangular lens at 560 kHz. SPL difference is negative.

4. DISCUSSION

The focusing of acoustic waves in the second transmission band of a phononic crystal presents difficulties to the anisotropic scattering effects resulting from the wavelength of the impinging wave being on the same order as the lattice parameters. Many phononic crystal based lenses utilize a form of gradient indices to achieve focusing, but are restricted to operation in the first transmission band. For high frequency applications, the precise control of the distribution of materials necessary in a metamaterial lens makes practical realization difficult. Effective focusing and collimating of sound in the second band presents an advantageous opportunity to reduce this fabrication burden as it allows for larger structures to focus waves on the same order as the lattice spacing. This work has demonstrated the capability of a metamaterial lens to focus and collimate a small set of frequencies in the second transmission band of a simple, square lattice phononic crystal by geometric design of the lens. Frequency sensitivity ranged from $\pm < 2.5 \, kHz$ for the hemisphere lens, to $\pm < 1.5 \, kHz$ for the triangular arrowhead lens.

5. REFERENCES

[1] V. Veselago, "The electrodynamics of substances with simultaneously negative values of permittivity and permeability," *Sov Phys Uspekhi,* vol. 10, no. 4, 1968.

[2] G. Eleftheriades, "EM transmission-line metamaterials," *Materials Today,* vol. 12, no. 3, 2009.

[3] P. Bhattacharya, J. Sabarinathan, J. Topolancik, S. Chakravarty, P. Yu and W. Zhou, "Quantum Dot Photonic Crystal Light Sources," *Proceedings of the IEEE,* vol. 93, no. 10, 2005.

[4] D. Krishnan and H. Johnson, "Optical properties of two-dimensional polymer photonic crystals after deformation-induced pattern transformations," *Journal of the Mechanics and Physics of Solids,* vol. 57, pp. 1500-1513, 2009.

[5] J. Vuckavoic and Y. Yamamoto, "Photonic crystal microcavities for cavity quantum electrodynamics with a single quantum dot," *Applied Physics Letters,* vol. 82, no. 15, 2003.

[6] P. Russell, Photonic crystal fibers: Basics and applications, Erlangen, Germany: Elsevier Inc., 2008.

[7] J. B. Pendry, "Negative Refraction Makes a Perfect Lens," *Physical Review Letters,* vol. 85, no. 18, pp. 3966-3969, 2000.

[8] W. Cai, U. Chettiar, A. Kildishev and V. Shlaev, "Optical cloaking with metamaterials," *Nature Photonics,* vol. 1, pp. 224-227, 2007.

[9] K. Aydin, I. Bulu and E. Oabay, "Subwavelength resolution with a negative-index metamaterial superlens," *Applied Physics Letters,* vol. 60, no. 254102, 2004.

[10] N. Fang and X. Zhang, "Imaging properties of a metamaterial superlens," *Applied Physics Letters,* vol. 82, no. 161, 2003.

[11] H. E. Moses, R. J. Nagem and G. v. H. Sandri, "The general solution of the three dimentsional acoustic equation and of Maxwell's equations in the infinite domain in terms of the asymptotic solution in the wave zone," *Journal of Mathematical Physics,* vol. 33, no. 86, 1992.

[12] M. Kushwaha, P. Halevi and G. Martinez, "Theory of acoustic band structure of periodic elastic composites," *Physical Review B,* vol. 49, no. 4, 1994.

[13] S. Peng, C. Qiu, Z. He, Y. Ye, S. Xu, K. Tang, M. Ke and Z. Liu, "Extraordinary acoustic shielding by a monolayer of periodical polymethyl methacrylate cylinders immersed in water," *Journal of Applied Physics,* vol. 110, no. 014509, 2011.

[14] S. Zhang, C. Xia and N. Fang, "Broadband Acoustic Cloak for Ultrasound Waves," *Physical Review Letters,* vol. 106, no. 024301, 2011.

[15] A. Sukhovich, B. Merheb, K. Muralidharan, J. Vasseur, Y. Pennec, P. Deymier and J. Page, "Experimental and Theoretical Evidence for Subwavelength Imaging in Phononic Crystals," *Physical Review Letters,* vol. 102, no. 154301, 2009.

[16] J.-F. Robillard, J. Bucay, P. Deymier, A. Shelke, K. Muralidharan, B. Merheb, J. Vasseur, A. Sukhovich and J. Page, "Resolution limit of a phononic crystal superlens," *Physical Review B,* vol. 83, no. 224301, 2011.

[17] J. Bucay, E. Roussel, J. O. Vasseur, P. A. Deymier, A.-C. Hladky-Hennion, Y. Pennec, K.

Muralidharan, B. Djafari-Rouhani and B. Dubus, "Positive, negative, zero refraction, and beam splitting in a solid/air phononic crystal: Theoretical and experimental study," *Physical Review B,* vol. 79, no. 214305, 2009.

[18] M.-H. Lu, L. Feng and Y.-F. Chen, "Phononic crystals and acoustic metamaterials," *Materials Today,* vol. 12, no. 12, 2009.

[19] Y. Wu and Z.-Q. Zhang, "Dispersion relations and their symmetry properties of electromagnetic and elastic metamaterials in two dimensions," *Physical Review B,* vol. 79, no. 195111, 2009.

[20] P. Halevi, A. A. Krokhin and J. Arriaga, "Photonic crystal optics and homogenization of 2D periodic composites," *Phys. Rev. Lett.,* vol. 82, pp. 719-722, 1999.

[21] A. Krokhin, J. Arriaga and L. N. Gumen, "Speed of Sound in Periodic Elastic Composites," *Physical Review Letters,* vol. 91, no. 26, 2003.

[22] M. Centini, C. Sibilia, M. Scalora, G. Aguanno, M. Bertolotti, M. J. Bloemer, C. Bowden and I. Nefedov, "Dispersive properties of finite, one-dimensional photonic band gap structures: Applications to nonlinear quadratic interactions," *Physical Review E,* vol. 60, no. 4, 1999.

[23] C. Luo, S. Johnson, J. Joannopoulos and J. Pendry, "All-angle negative refraction without negative effective index," *Physical Review B,* vol. 65, no. 201104, 2002.

[24] T.-Y. Chiang, L.-Y. Wu, C.-N. Tsai and L.-W. Chen, "A multilayered acoustic hyperlens with acoustic metamaterials," *Applied Physics A,* vol. 103, pp. 355-359, 2011.